Malaysian Journal of Mathematical Sciences 18(4): 755–774 (2024)
https://doi.org/10.47836/mjms.18.4.05

Malaysian Journal of Mathematical Sciences

Journal homepage: https://mjms.upm.edu.my

Mathematical Fractional Analysis on Blood Casson Fluid in Slip and Small Arteries with the Cholesterol Porosity Effect

Azmi, W. F. W.[1], Mohamad, A. Q.*[1], Jiann, L. Y.[1], and Shafie, S.[1]

[1]*Department of Mathematical Sciences, Faculty of Science, Universiti Teknologi Malaysia, 81310 UTM Johor Bahru, Johor, Malaysia*

E-mail: ahmadqushairi@utm.my
**Corresponding author*

Received: 25 November 2023
Accepted: 18 July 2024

Abstract

Studying human blood flow is crucial in biomedical research to address blood-related disorders. However, experimental studies are costly and time-consuming. Hence, mathematical models have been developed to represent these physical phenomena. Yet, existing models often overlook the slip boundary effect. This study explores an analytical solution for the pulsatile flow of a fractional Casson fluid in a slip cylinder, considering free convection, magnetic fields, and porosity. Employing the Caputo–Fabrizio fractional derivative method, the problem is modelled. Analytical solutions are obtained using Laplace and finite Hankel transforms. Graphical representations illustrate velocity and temperature profiles, emphasizing parameters such as magnetic, Casson, Darcy, fractional, slip, Grashof, and Prandtl numbers. Numerical results for skin friction and Nusselt number are tabulated. The results suggest that enhanced slip velocity amplifies fluid flow, particularly near the cylinder's surface, generating lubrication to alleviate blood-vessel friction and improve blood flow by enabling smoother movement along vessel walls. The fractional-order derivative fluid model is more practical and realistic compared to the classical fluid model due to its memory effect which sudden rise in blood velocity can potentially damage the blood vessel and lead to atherosclerosis. The obtained analytical result can be used to validate the accuracy of the mathematical model obtained by numerical methods.

Keywords: blood Casson fluid; Caputo–Fabrizio fractional derivative; heat transfer; Hankel transform; slip velocity.

1 Introduction

The latest developments in industrial sectors, such as generators, wastewater treatment, and drug delivery in human blood, emphasize the growing interest among researchers [14]. Chamkha et al. [15] stated that among the three heat transfer mechanisms, free, force, and mixed convection, free convection typically garners significant focus, as study by Jha et al. [30]. Dehbani et al. [19] defined free convection as one of the forms of heat transportation that involves the interaction between buoyancy and gravitational force, which arises because of the density change caused by a temperature gradient. It is significant for energy conservation since it requires no energy absorbers, as highlighted by Husain et al. [25]. Motivated by it, Khan et al. [32] considered the free convection effect on the viscous fluid behaviour in an oscillating cylinder. They obtained the result that this phenomenon enhanced fluid flow and obtained the analytical result by combining the Laplace and Hankel transform methods. Then, Javaid et al. [29] extended a similar problem to Khan et al. [32] to study second-grade fluid behaviour, and they obtained the same analytical result with the same methods.

One of the heat transfer sources is Magnetohydrodynamics (MHD), which arises from the induced current generated when an electrically conducting fluid flows through an applied magnetic field. It can be found in the metallurgical industry and treats cancer in biomedical applications [22]. Abdelhameed [3] explored the MHD and free convection impacts on the water flow, which is Newtonian fluid through an accelerated plate. He employed the Laplace transform approach to obtain the exact result. He highlighted that MHD causes fluid velocity to decline. Anuraq et al. [9] extended a similar problem reported by Abdelhameed [3], which is the flow between two fixed cylinders. Comparable results were achieved by applying the Laplace and finite Hankel transform to the analytical solution.

Moreover, a porous medium is another technique to enhance convective heat transfer properties, as stated by Xu et al. [56]. Mahdi et al. [36] and Khaled et al. [31] defined a porous medium as any material that encompasses a solid matrix and interconnected voids. Examples of porous media include rocks, cells, the cholesterol effect, fatty plaque, and others, as mentioned by Dash et al. [18]. In the investigation of pulsatile blood flow within a porous medium, Elshehawey [20] were early researchers who derived an analytical solution for Newtonian fluid. They employed the Laplace and finite Hankel transforms to address this particular challenge. Then, Rathod et al. [49] discovered a similar issue and method as Elsehawey et al. [20] for non-Newtonian fluid by adding the MHD effect. They found that fluid velocity rises in direct proportion to the porous medium's permeability. Anurag et al. [10] investigated analytically the porosity impact on the viscous fluid, which is moving freely in the fixed cylinder by convection, and obtained similar results as Rathod et al. [49].

Besides, most studies have assumed non-slip conditions for the fluid flow problem. In fluid mechanics studies, the prevailing hypothesis suggests that fluid adhering to the boundary is proven effective for Newtonian fluid flow only. Rao et al. [47] defined slip as the finite velocity between fluid flow particles and a solid boundary. It is observed in practical scenarios such as blood flow in elastic arteries and oil suspension flow in pipelines, as emphasized by Nubar et al. [44]. Encouraged by it, Abd El-Aziz et al. [1] analyzed the slip boundary's impact on the plate for the flow characteristics of Newtonian and non-Newtonian fluids (Casson fluid). They obtained the semi-analytical result by using the perturbation technique. The existence of the slip can reduce the friction force, which enhances the fluid velocity. Padma et al. [46] studied how slip and non-slip conditions impact the flow characteristics of Jefrey fluid model, specifically in blood flow within a stenosed artery, considering the MHD effect. Then, Padma et al. [45] extended this study by incorporating additional effects of body acceleration and an external electric field. Both studies

addressed these issues analytically by employing Laplace and finite Hankel transforms for their solution. Studies have indicated that the existence of a slip boundary leads to an increase in the velocity of fluid flow. Then, Nandal et al. [42] created a mathematical model to represent pulsating blood flow in the stenotic cylinder with a slip condition present. They obtained similar analytical results by using the same methods as Padma et al. [46]. More discussions on the impact of slip boundaries can be found in the references. For instance, Yanala et al. [58] examined the numerical effects of slip conditions on a plate, considering the impact of chemical reactions and thermal radiation. Subba Rao et al. [48] studied the numerical effects of slip on Powell-Eyring fluid over a radially stretching surface. Choudhari et al. [17] investigated the impact of slip conditions on Herschel-Bulkley fluid flow in a tube, and this study was subsequently extended by Baliga et al. [11] to include thermal slip in an inclined tube.

Fluid is one of the heat carriers involved in the cooling and heating processes. The Casson fluid has been extensively investigated as a non-Newtonian fluid in academic research. It exhibits elastic solid behaviour when the yield stress exceeds the applied shear stress, while fluid starts to flow if the shear stress condition is reversed, as defined by Sochi [55] and Alderman [4]. According to Chhabra [16], due to its unique characteristics, this fluid exhibits potential suitability as an approximation for biological fluids, such as human blood. As indicated by Sankar and Ismail [52], the Casson fluid model is suitable for analyzing blood flow behaviour in small arteries ranging from 130 to 1300 μm in diameter. Hayat et al. [23] revealed the flow characteristics of Casson fluids occurring at the stagnation point of the stretching cylinder. They applied the Homotopy analysis approach and obtained that increasing the Casson parameter caused a more significant fluid velocity as close to the cylinder's wall and a lesser one as it was farther away. Later, Jalil et al. [26] delved into the behaviour of a Casson fluid experiencing free convection within a stretching cylinder. The Keller box approach was utilized to find the numerical answer. Conversely, Kumar et al. [35] observed an augmentation in fluid velocity due to the Casson parameter in the moving cylinder. They obtained numerical results by using the Crank-Nicolson method. Due to the differences in the time interval, Kumar et al. [35] evaluated the result for a small interval, while Jalil et al. [26] analyzed the result for a more significant time interval. Another explanation of the.

Recently, researchers have been attracted to employing fractional derivatives in the governing equation since they are more realistic and accurate than the classical model [54]. Moreover, it is extensively used in engineering and industrial applications, such as signal processing, as stated by Ray et al. [50] and in biological practices like cancer treatment and drug delivery, as noted by Faraloya et al. [21]. Ali et al. [8] adopted the Caputo fractional derivative as a mathematical tool for characterizing the momentum equation in the context of Casson fluid flow within a stationary cylinder influenced by magnetohydrodynamics (MHD). To address the problem, the Hankel and Laplace transforms were used. The results indicate that fractional parameters can increase or decrease fluid velocity depending on the temporal factors. Later, Sene [53] applied the previously mentioned fractional operator to investigate natural convection flow over a mobile plate within the framework of the Casson fluid model. They used the Laplace transform to solve analytically and obtained the same result as Ali et al. [8]. Moitoi et al. [41] examined blood behaviour as Newtonian fluid flow in a permeable cylinder with the effect of body acceleration. Bayissa Yadeta et al. [57] extended this study to consider blood flow as a Casson fluid in the cylinder, incorporating the effects of MHD. They employed the Caputo fractional derivative and obtained semi-analytical solutions.

Subsequently, the Caputo-Fabrizio fractional derivative can effectively overcome the limitations of representing physical phenomena [12]. Examining a Casson fluid, Ali et al. [5] scrutinized the characteristics of magnetic particles confined within a stationary cylinder. The fractional derivative method of Caputo–Fabrizio was applied. They devised an analytical answer using the same approach as Ali et al. [8]. They found that a fractional parameter controls fluid velocity.

Ali et al. [6] extended the same problem and obtained the same results as Ali et al. [5] with a moving cylinder. Later, Ali et al. [7] studied a similar problem as Ali et al. [5], which involves flow in an oscillating cylinder without considering magnetic particles. The study presents evidence supporting the fractional fluid model's enhanced fidelity compared to the classical fluid model. Furthermore, Maiti et al. [37] examined the Casson fluid flow in a stationary cylinder, considering the effects of body acceleration, MHD, thermal radiation, and porous medium. Subsequently, Maiti et al. [38] extended the problem by incorporating the additional effect of chemical reactions. Later, Maiti et al. [39] extended the study to include the involvement of magnetic particles. They used the Caputo-Fabrizio fractional derivative approach. When controlling the thermal behaviour of fluids, the fractional parameter is essential. In addition, the effect of the fractional parameter on MHD Casson fluid flow with magnetic particles in an inclined cylinder with radially non-symmetric geometrical stenosis was investigated by Jamil et al. [27] while the effect with multi-stenosis was explored by Jamil et al. [28]. They mentioned that fractional derivatives have a memory effect and are controllers of fluid velocity. The problem was analytically solved by combining Laplace and finite Hankel transforms. All researchers assumed a no-slip boundary condition in their fractional derivative problems.

Past literature has addressed slip velocity's impact on non-Newtonian fluids (Jeffrey fluid, Herschel-Bulkley fluid) to simulate arterial blood flow, yielding semi-analytical and analytical solutions. However, no analytical solution has been provided for Casson fluid flow in the cylinder with slip velocity effects which focused on the human blood properties in the diameter range of 130 to 1300 μm. Moreover, most researchers used the Caputo-Fabrizio fractional derivative method without considering slip velocity effects, resulting in analytical solutions with special functions that cannot be directly plotted. This study's novelty lies in obtaining an analytical solution in closed form without special functions, serving as a benchmark for numerical solutions and analyzing the impact of slip velocity on the fractional Casson fluid model. This study also examined the effects of MHD, pulsatile pressure gradient, porous medium (cholesterol effect), and free convection flow. Incorporating the slip boundary condition of the cylinder enables accurate modelling, especially in biomedical contexts where Casson fluid represents blood flow in constricted vessels. The study achieves its objectives by transforming governing equations into a dimensionless form and employing the Caputo-Fabrizio fractional derivative model. Analytical solutions for velocity and temperature profiles are obtained through Laplace and finite Hankel transforms, visualized using the Maple program.

2 Problem Formulation

The depiction of the porous medium in the context of MHD Casson fluid flow within a horizontal cylinder is visually explained in Figure 1, where the radius is denoted as r_0. The pulsatile pressure gradient is responsible for initiating this fluid motion. The free convection and slip velocity effects are considered in this approach. Given that the cylinder's fluid flow is considered, the fluid flow problem will be investigated in the cylindrical polar coordinate. In the Casson fluid flow context, the z-axis delineates fluid motion direction, whereas the r-axis remains orthogonal to the cylinder's horizontal axis. This investigation scrutinizes the utilization of B_0, representing magnetic field intensity, concerning the radial coordinate. Assuming that the induced magnetic field produced by fluid flow is negligible due to a very small Reynolds number, as highlighted by Kumar et al. [34] and the Hall effect in magnetohydrodynamics is considered insignificant, as stated by Krishna et al. [33]. Besides that, the porous medium inertia effects are disregarded due to the low flow velocities, and the local thermal equilibrium condition is applied to simplify the mathematical formulation [13]. The function describing fluid velocity and temperature is as-

sumed to depend solely on the variables r and t. At t^*=0, both the Casson fluid and the cylinder are in a state of idleness, characterized by the ambient temperature, T_∞. Upon reaching $t^* > 0$, the fluid initiates its motion, featuring a slip velocity at the cylinder wall's surface. Concurrently, the cylinder's temperature increases from the ambient temperature marked as T_∞ to match the wall's temperature, labelled as T_w, and remains constant, as shown in Figure 1.

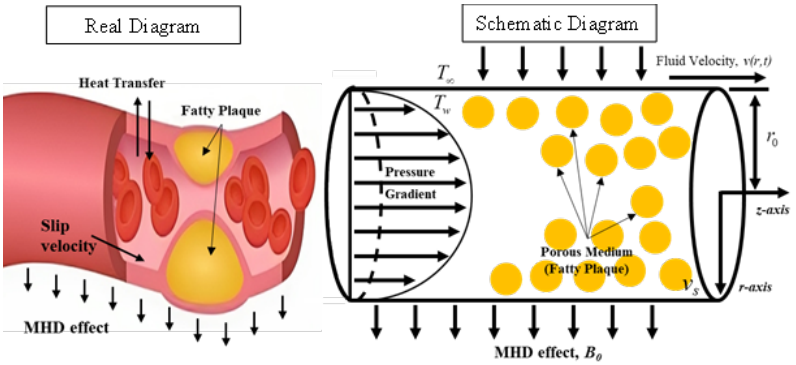

Figure 1: The graphical depiction of the fluid flow phenomenon.

The governing equations for this study are based on the conservation laws of mass, linear momentum and energy in the cylinder, which had been formulated by considering factors such as free convection flow, magnetic field, porous medium, and the influence of a pulsating pressure gradient. These equations are derived within the framework of the earlier mentioned assumptions and by applying Boussinesq's approximation [7, 37], which yield momentum Casson and energy equations as;

$$\rho\frac{\partial v^*}{\partial t^*} = -\frac{\partial p^*}{\partial z^*} + \mu\left(1+\frac{1}{\zeta}\right)\left(\frac{\partial^2 v^*}{\partial r^{*2}} + \frac{1}{r^*}\frac{\partial v^*}{\partial r^*}\right) - \frac{\mu}{k_p}v^* - \sigma B_0^2 v^* + g\rho\beta_t(T-T_\infty), \tag{1}$$

$$\rho c_p\frac{\partial T^*}{\partial t^*} = k\left(\frac{\partial^2 T^*}{\partial r^{*2}} + \frac{1}{r^*}\frac{\partial T^*}{\partial r^*}\right), \tag{2}$$

where the density of fluid (ρ), the z-axis velocity component (v^*), a pulsatile pressure gradient $(\partial p^*/\partial z^*)$, dynamic viscosity (μ), the non-Newtonian Casson parameter $(\zeta = \mu_B\sqrt{2\pi_c}/\tau_y)$, permeability constant (k_p), electrical conductivity (σ), applied magnetic field strength (B_0), gravitational acceleration (g), coefficient of thermal expansion (β_T), fluid temperature (T), specific heat capacity at constant temperature (c_p), and thermal conductivity (k). Subsequently, the initial and boundary conditions relevant to this problem are presented [32, 46];

$$\begin{aligned} v^*(r^*,0) &= 0, \qquad T(r^*,0) = T_\infty, \qquad ; r \in [0, r_0], \\ v^*(r_0,t^*) &= v_s^*, \qquad T(r_0,t^*) = T_w, \qquad ; t^* > 0, \end{aligned} \tag{3}$$

where v_s is slip velocity. Showcasing the relevant dimensionless variables [32, 45];

$$t = \frac{t^*\nu}{r_0^2}, \quad r = \frac{r^*}{r_0}, \quad v = \frac{v^*}{v_0}, \quad v_s = \frac{v_s^*}{v_0}, \quad z = \frac{z^*}{z_0}, \quad p = \frac{p^* r_0}{\mu v_0}, \quad \theta = \frac{T-T_\infty}{T_w - T_\infty}. \tag{4}$$

In conjunction with the initial and boundary conditions (3) and the governing equations for momentum (1) and energy (2), transform them into a dimensionless form using dimensionless variables (4) and obtain the following;

$$\frac{\partial v}{\partial t} = -\frac{\partial p}{\partial z} + \zeta_1\left(\frac{\partial^2 v}{\partial r^2} + \frac{1}{r}\frac{\partial v}{\partial r}\right) - \frac{1}{Da}v - Mv + Gr\theta, \tag{5}$$

$$\frac{\partial \theta}{\partial t} = \frac{1}{\mathrm{Pr}} \left(\frac{\partial^2 \theta}{\partial r^2} + \frac{1}{r} \frac{\partial \theta}{\partial r} \right), \tag{6}$$

with the conditions

$$\begin{aligned} v(r,0) &= 0, \qquad \theta(r,0) = 0, \qquad ; r \in [0,1], \\ v(1,t) &= v_s, \qquad \theta(1,t) = 1, \qquad ; t > 0, \end{aligned} \tag{7}$$

where the obtained dimensionless parameters are as follows: Darcy number $Da = \frac{k_p}{r_0^2}$, magnetic parameter $M = \frac{\sigma r_0^2 B_0^2}{\mu}$, Grashof number $Gr = \frac{g\beta_T (T_w - T_\infty) r_0^2}{\nu u_0}$, and Prandtl number $Pr = \frac{\mu c_p}{k}$, Meanwhile, $\zeta_1 = \frac{1}{\zeta_0}$ and $\zeta_0 = 1 + \frac{1}{\zeta}$ are the constant parameters, and $\zeta = \mu_B \sqrt{2\pi_c}/\tau_y$ is the Casson parameter. The pulsatile pressure gradient replicates the cyclic pumping mechanism of the heart [37], which is $-\frac{\partial p}{\partial z} = A_0 + A_1 \cos(\omega t)$ where A_0 and A_1 are the constants of pulsatile amplitude, ω defined as the pulsatile frequency. The dimensionless momentum governing equation can be written as,

$$\frac{\partial v}{\partial t} = A_0 + A_1 cos(\omega t) + \zeta_1 \left(\frac{\partial^2 v}{\partial r^2} + \frac{1}{r} \frac{\partial v}{\partial r} \right) - \frac{1}{Da} v - Mv + Gr\theta. \tag{8}$$

By applying the Caputo-Fabrizio fractional derivative, the time derivative on the left-hand side of (6) and (8) is transformed into its fractional form, which yields [37],

$${}^{CF}D_t^{\alpha} v(r,t) = A_0 + A_1 cos(\omega t) + \zeta_1 \left(\frac{\partial^2 v}{\partial r^2} + \frac{1}{r} \frac{\partial v}{\partial r} \right) - \frac{1}{Da} v - Mv + Gr\theta, \tag{9}$$

$${}^{CF}D_t^{\alpha} \theta(r,t) = \frac{1}{\mathrm{Pr}} \left(\frac{\partial^2 \theta}{\partial r^2} + \frac{1}{r} \frac{\partial \theta}{\partial r} \right), \tag{10}$$

where ${}^{CF}D_t^{\alpha} f(r,t) = \frac{1}{1-\alpha} \int_0^{\tau} \exp\left(\frac{-\alpha(\tau - t)}{1-\alpha} \right) f'(\tau)\, dt$, $0 < \alpha < 1$ is the definition of the non-singular kernel Caputo-Fabrizio fractional derivative and α is a fractional derivative parameter [37].

3 Problem Solution

The study examines heat transfer and the movement of MHD Casson fluid within a porous medium inside a cylinder with slip conditions. This investigation's analysis utilizes Laplace transform and finite Hankel transform methodologies. A fluctuating pressure gradient drives this setup. The Laplace transform is a frequently used mathematical method for addressing issues associated with initial boundary values and transient scenarios. While dealing with cylindrical domains, the finite Hankel transform offers unique advantages. The process of reducing a partial differential equation results in the appearance of an ordinary differential equation. The analytical outcome will be derived by employing the inverse of both methodologies.

3.1 Calculation of temperature

Modifying (10) and their associated initial and boundary conditions (7) is achieved through the application of the Laplace transform technique. This transformation leads to

$$\frac{a_0 q\,\bar{\theta}(r,q)}{q+a_1} = \frac{1}{\mathrm{Pr}}\left(\frac{\partial^2\bar{\theta}(r,q)}{\partial r^2} + \frac{1}{r}\frac{\partial\bar{\theta}(r,q)}{\partial r}\right), \tag{11}$$

$$\bar{\theta}(1,q) = \frac{1}{q}, \tag{12}$$

where the fractional constant parameters representing as $a_0 = 1/1-\alpha$ and $a_1 = a_0\alpha$, the Laplace transform of the function $\theta(r,t)$ is indicated by $\bar{\theta}(r,q)$, and q is the transformation variable. Next, (11) undergoes the zero-order finite Hankel transform while incorporating condition (12). The outcome is as follows,

$$\bar{\theta}_H(r_n,q) = \frac{r_n J_1(r_n)}{q}\left[\frac{q+a_1}{(a_0\mathrm{Pr}+r_n^2)q+a_1 r_n^2}\right], \tag{13}$$

where $\bar{\theta}_H(r,q) = \int_0^1 r\bar{\theta}(r,q)J_0(rr_n)dr$ is the finite Hankel transform of the function $\bar{\theta}(r,q)$ and r_n with $n = 0,1,\ldots$ are the positive roots of the equation $J_0(x) = 0$, where J_0 represents the Bessel function of the first kind with zero-order, and J_1 signifies the Bessel function of the first kind with first-order. Subsequently, (13) is further simplified and derived as follows,

$$\bar{\theta}_H(r_n,q) = \frac{J_1(r_n)}{r_n}\left[\frac{1}{q} - \frac{a_0\mathrm{Pr}}{(q+a_3[n])(a_0\mathrm{Pr}+r_n^2)}\right], \tag{14}$$

where $a_3[n] = a_1 r_n^2/(a_0\mathrm{Pr}+r_n^2)$ is the constant parameter. Subsequently, (14) undergoes the inverse Laplace transform, resulting in

$$\theta_H(r_n,t) = \frac{J_1(r_n)}{r_n}\left[1 - \frac{a_0\,\mathrm{Pr}\exp(-a_3[n]t)}{a_0\,\mathrm{Pr}+r_n^2}\right]. \tag{15}$$

Lastly, we attain an analytical expression for the temperature profiles, (15), by employing the inverse finite Hankel transform, resulting in

$$\theta(r,t) = 1 - 2a_0\,\mathrm{Pr}\sum_{n=1}^{\infty}\frac{J_0(rr_n)\exp(-a_3[n]t)}{r_n J_1(r_n)(a_0\mathrm{Pr}+r_n^2)}. \tag{16}$$

3.2 Calculation of velocity

Utilizing the Laplace transform on (9) in combination with the relevant initial and boundary conditions (7) produces the resulting expression

$$\begin{aligned}\frac{a_0\,q\bar{v}(r,q)}{q+a_1} = \frac{A_0}{q} + \frac{A_1\,q}{q^2+\omega^2} + \zeta_1\left(\frac{\partial^2\bar{v}(r,q)}{\partial r^2} + \frac{1}{r}\frac{\partial\bar{v}(r,q)}{\partial r}\right)\\ - \frac{1}{Da}\bar{v}(r,q) - M\bar{v}(r,q) + Gr\bar{\theta}(r,q),\end{aligned} \tag{17}$$

$$\bar{v}(1,q) = \frac{v_s}{q}, \tag{18}$$

representing the Laplace transform of the function $v(r,t)$, $\bar{v}(r,q)$ is identified. Next, Laplace's partial differential equation, (17), in conjunction with the boundary conditions, (18), transforms

an ordinary differential equation (ODE) using the zero-order finite Hankel transform method, resulting in

$$\bar{v}_H(r_n,q)=\frac{J_1(r_n)}{r_n}\left(\frac{A_0}{q}+\frac{A_1\,q}{q^2+\omega^2}+\zeta_1 r_n^2\frac{v_s}{q}+Gr\bar{\theta}(r_n,q)\right)\left(\frac{q+a_1}{(a_0+A_3[n])q+a_1\,A_3[n]}\right), \quad (19)$$

where $\bar{v}_H(r,q)=\int_0^1 r\bar{v}(r,q)J_0(rr_n)\,dr$ is the finite Hankel transform of the function $\bar{v}(r,q)$, and $A_3[n]=M+\dfrac{1}{Da}+\zeta_1 r_n^2$ is a constant parameter. In (19) is subjected to the inverse Laplace transform in the following step, resulting in

$$v_H(r_n,t)=v_1(t)+v_2(t)+v_3(t)+v_4(t)-v_5(t), \quad (20)$$

with

$$\begin{aligned}
v_1(t)&=\frac{J_1(r_n)}{r_n}\frac{A_0}{A_3[n]}\left(1-\frac{a_0}{L[n]}\exp(-J[n]t\right),\\
v_2(t)&=\frac{J_1(r_n)}{r_n}\frac{A_1}{L[n](\omega^2+J[n]^2)}((\omega^2+a_1J[n])\cos(\omega t)-(\omega J[n]-a_1\omega)\sin(\omega t)\\
&\quad -J[n](a_1-J[n])\exp(-J[n]t)),\\
v_3(t)&=\frac{J_1(r_n)}{r_n}v_s\left[1-\frac{a_0\exp(-J[n]t}{L[n]}\left(1-\frac{a_3}{a_3+\zeta_1 r_n^2}\right)-\frac{a_3}{a_3+\zeta_1 r_n^2}\right],\\
v_4(t)&=\frac{J_1(r_n)}{r_n}\frac{Gr}{A_3[n]}\left[1-\frac{a_0}{L[n]}\exp(-J[n]t)\right],\\
v_5(t)&=\frac{J_1(r_n)}{r_n}\frac{Gr\,a_0\,\mathrm{Pr}}{(A_3[n]\mathrm{Pr}-r_n^2}\left[\frac{\mathrm{Pr}\exp(-H[n]t)}{a_0\mathrm{Pr}+r_n^2}-\frac{\exp(-J[n]t)}{L[n]}\right],
\end{aligned}$$

where $a_3=\dfrac{1}{Da}+M$, $J[n]=\dfrac{a_1A_3[n]}{a_0+A_3[n]}$, $L[n]=a_0+A_3[n]$ and $H[n]=\dfrac{a_1r_n^2}{a_0\mathrm{Pr}+r_n^2}$ are constant parameters. The inverse finite Hankel transform is applied to analytically solve (20) for the velocity profiles, resulting in the following expression,

$$\begin{aligned}
v(r,t)=v_s&-2a_0v_s\sum_{n=1}^{\infty}\frac{J_0(rr_n)}{r_nJ_1(r_n)}\frac{\exp(-J[n]t)}{L[n]}\left(1-\frac{a_3}{A_3[n]}\right)-2v_s\sum_{n=1}^{\infty}\frac{J_0(rr_n)}{r_nJ_1(r_n)}\frac{a_3}{A_3[n]}\\
&+2\sum_{n=1}^{\infty}\frac{J_0(rr_n)}{r_nJ_1(r_n)}\left[\frac{A_0}{A_3[n]}\left(1-\frac{a_0\exp(-J[n]t)}{L[n]}\right)\right]\\
&+2\sum_{n=1}^{\infty}\frac{J_0(rr_n)}{r_nJ_1(r_n)}\left[\frac{A_1}{L[n](J[n]^2+\omega^2)}\left(\omega^2+a_1J[n]\right)\cos(\omega t)-(\omega J[n]-a_1\omega)\sin(\omega t)\right]\\
&-J[n](a_1-J[n])\exp(-J[n]t)\\
&+2Gr\sum_{n=1}^{\infty}\frac{J_0(rr_n)}{r_nJ_1(r_n)}\left[\frac{1}{A_3[n]}+\frac{a_0\exp(-J[n]t)}{L[n]}\left(\frac{r_n^2}{A_3[n](A_3[n]\mathrm{Pr}-r_n^2)}\right)\right.\\
&\left.-\frac{a_0\mathrm{Pr}^2\exp(-H[n]t)}{(a_0\,\mathrm{Pr}+r_n^2)(A_3[n]\mathrm{Pr}-r_n^2)}\right].
\end{aligned} \quad (21)$$

3.3 Special case for classical fluid model ($\alpha = 1$)

When the fractional parameter $\alpha = 1$, the analytical solution for fluid temperature in the classical fluid model can be derived as,

$$\theta(r,t) = 1 - 2\sum_{n=1}^{\infty} \frac{J_0(rr_n)}{r_n J_1(r_n)} \exp\left(\frac{-r_n^2}{\mathrm{Pr}} t\right), \tag{22}$$

and the analytical solution of fluid velocity in the classical fluid model is obtained as,

$$v(r,t) = v_s + 2\sum_{n=1}^{\infty} \frac{J_0(rr_n)}{r_n J_1(r_n)} \Big[- v_1(r,t) + v_2(r,t) + v_3(r,t)\Big], \tag{23}$$

with

$$v_1(r,t) = v_s\left(\exp(-A_3[n]t) + \frac{a_3(1-\exp(-A_3[n]t))}{a_3 + \zeta_1 r_n^2}\right),$$

$$v_2(r,t) = \frac{A_0}{A_3[n]}\left(1 - \exp(-A_3[n]t) + \frac{A_1}{A_3[n]^2 + \omega^2}\left(\omega\sin(\omega t) + A_3[n]\Big(\cos(\omega t) - \exp(-A_3[n]t)\Big)\right)\right),$$

$$v_3(r,t) = Gr\left(\frac{1-\exp(-A_3[n]t)}{A_3[n]} - \frac{\mathrm{Pr}}{A_3[n]\mathrm{Pr} - r_n^2}\left(\exp\left(\frac{-r_n^2}{\mathrm{Pr}}t\right) - \exp(-A_3[n]t)\right)\right).$$

4 Nusselt Number and Skin Friction

Investigating the heat transfer rate and elucidating the connection between convective and conductive heat transfer are the goals of the Nusselt number calculation. It is shown by [7],

$$Nu = -\frac{\partial\theta(r,t)}{\partial r}\bigg|_{r=1}. \tag{24}$$

The skin friction is evaluated as the friction force or shear force applied to the surface of the cylinder, which is given as

$$\tau = -\left(1 + \frac{1}{\zeta}\right)\left[\frac{\partial v(r,t)}{\partial r}\right]_{r=1}. \tag{25}$$

5 Results and Discussion

To guarantee that the analytical solution (21) is accurate, compare the limiting case of the acquired outcome to the prior finding by [32]. Both graphs are aligned based on the observation, indicating that they are in accord with one another. Hence, it is agreed that the analytical solution (21) is accurate, as shown in Figure 2.

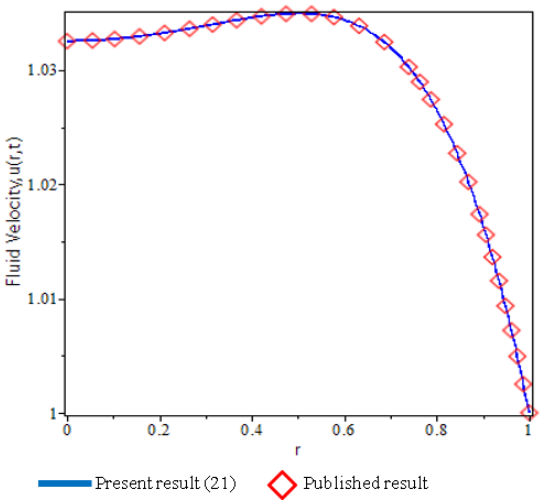

Figure 2: Evaluation of fluid velocity $v(r,t)$ in (21) with $\zeta = Da = \infty$, $v_s = \alpha = 1.0$, $A_0 = A_1 = M = 0$, and in equation (29) with $\omega = 0$ by Khan et al. [32].

By using the key factors Casson parameter ζ, Magnetic parameter M, Darcy number Da, Grashof number Gr, Prandtl number Pr, slip velocity parameter v_s, fractional parameter α, and time parameter t, the blood flow properties of the fractional derivative model have been investigated and visually displayed in Figures 3 – 8. Additionally, Tables 1 and 2 provide the Nusselt number and skin friction. Based on the references, the parametric analysis is conducted using the following values: v_s =0 for no-slip conditions, Pr=21.0 for the Prandtl number representing blood, $t = 1.0$ for the initial state, $t = 10.0$ for the steady-state, $\zeta = 0.8$, $Gr = M = Da = 1.0$, $\alpha = 0.5$ and the significant parameter ranges are $\zeta = 0.4, 0.8, 1.2$, $Pr = 5.0, 7.2, 21$ [32, 46]. Additionally, for a comprehensive spectrum, some parameter values are approximated as follows: vs =0.2 for slip conditions, $Gr = M = Da = 1.0, 2.0, 3.0$, and $\alpha = 0.2, 0.5, 1.0$.

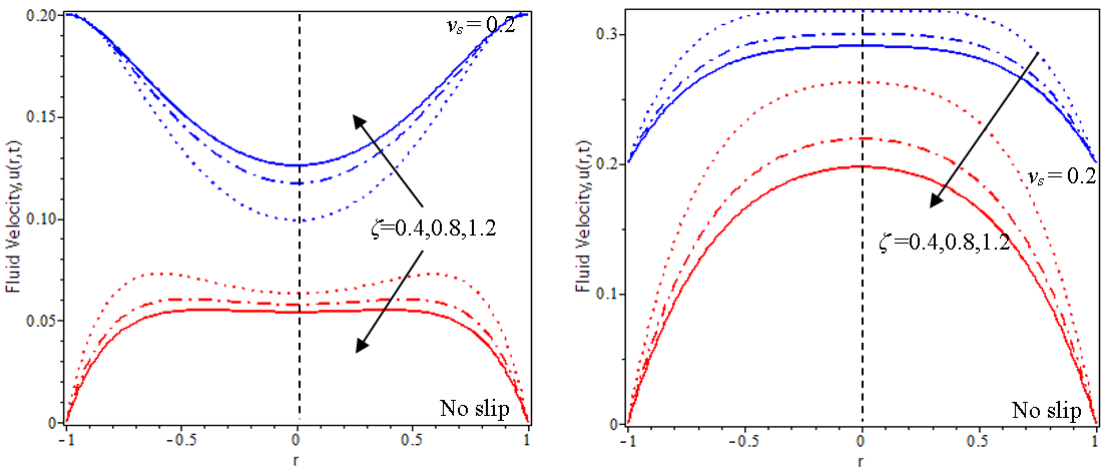

(a) t=1.0 (b) t=10.0

Figure 3: The result of the Casson parameter on the behavior of fluid velocity $v(r,t)$ when $\alpha = 0.5$, $A_0 = A_1 = 0.05$, $\omega = \pi/4$, $M = Da = Gr = 1$, and $\mathrm{Pr} = 21$.

Figure 3 demonstrates how the fluid velocity is influenced by conditions of slip and no-slip at the boundary, particularly about the Casson parameter,ζ. In general, Casson fluid behaves in a manner that replicates how human blood flows via narrow arteries [37]. During the short time interval $(t = 1.0)$, the slip effect induced by the Casson parameter results in an augmentation of fluid velocity. It causes a fall in the fluid's yield stress, which corresponds to the minimal force needed to start fluid flow. The introduction of slip velocity has a notable influence on the onset of fluid motion. As the Casson parameter increases, we can observe a reduction in fluid rate, considering the combined effects of slip and no-slip conditions over a substantial period $(t = 10.0)$. The reason is the increase of plastic dynamic viscosity, which causes the internal friction coefficient to rise. Thus, the shear thickening factor also rises, a force required to maintain a constant flow. It causes fluid viscosity to increase and fluid to become thicker. Additionally, the Casson parameter is significant in blood flow because it directly influences the velocity and viscosity, which can impact the blood circulatory system in small arteries ranging from 130 to $1300\mu m$ in diameter.

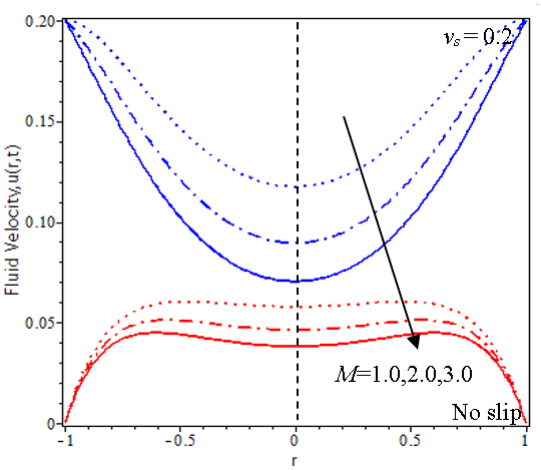

Figure 4: The result of Magnetic parameter on fluid velocity behavior $v(r,t)$ when $\alpha = 0.5$, $A_0 = A_1 = 0.05$, $\zeta = 0.8$, $\omega = \pi/4$, $Da = Gr = 1$, $\mathrm{Pr} = 21$, and $t = 1$.

This research investigates how applied magnetic fields impact the behaviour of fluid velocity, as illustrated in Figure 4. The study is centred on understanding the occurrence of slip and no-slip effects within the system. Current examination demonstrates that an increased magnetic parameter decreases fluid velocity in slip and no-slip scenarios. That is because the resistance force (Lorentz force) occurs when the applied magnetic field reacts with the induced current generated from moving electrical conducting fluid (human blood). Human blood comprises 55% plasma containing 91.5% water and 8.5% other solid components. One of the components is sodium, which can conduct electricity [2, 24]. Moreover, the magnetic field plays a crucial role in regulating blood circulation within the human body, influencing both the flow and viscosity of blood in the context of magnetic therapy or magnetotherapy.

The behaviour of fluid velocity with the porous medium effect in slip or no-slip conditions is presented in Figure 5. Demonstrating the increase in fluid velocity with the rise in the Darcy number (Da), which signifies the porous medium, is observed under both no-slip and slip conditions. The observed outcome can be attributed to a higher Darcy number, resulting in increased permeability of the porous medium. This phenomenon indicates the fluid's enhanced capacity to traverse through the porous medium. It can be described as blood flow in tiny capillaries with excess fat, cholesterol plaques, and blood clots [40]. It can be deduced that increased permeability

in porous mediums results in smoother blood flow within arteries by reducing flow resistance.

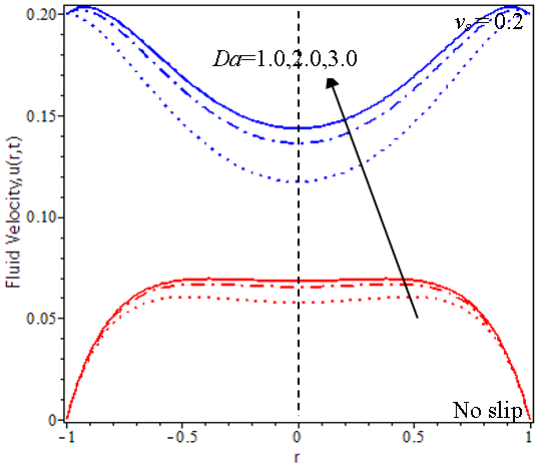

Figure 5: The result of Darcy number on fluid velocity behavior $v(r,t)$ when $\alpha = 0.5, A_0 = A_1 = 0.05, \omega = \pi/4, \zeta = 0.8, M = Gr = 1$, $\mathrm{Pr} = 21$, and $t = 1$.

In Figure 6, the impact of the thermal Grashof number on fluid velocity patterns is visually depicted, considering slip and no-slip conditions at the cylinder's wall. The graph illustrates that fluid velocity increases with the increment of the thermal Grashof number, a phenomenon observed in both slip scenarios. Since it is predominant during free convection flow, the thermal buoyancy force rises with the Grashof number. This phenomenon can be attributed to the naturally occurring variations in temperature and density within the fluid flow. An increase in fluid temperature leads to decreased fluid density, resulting in the upward movement of heated fluid due to the buoyancy effect. In contrast, cold fluid descends due to the influence of gravity. This leads to an upsurge in fluid velocity. In other words, the increased buoyancy forces compared to viscous forces accelerate blood flow, with significant implications for various physiological processes in the human body.

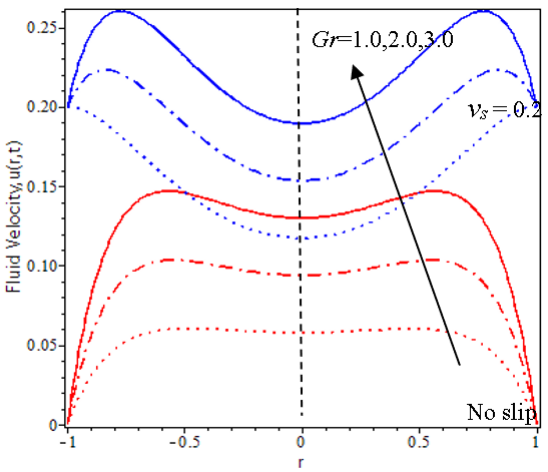

Figure 6: Result Thermal Grashof number on fluid velocity behaviour $v(r,t)$ when $\alpha = 0.5, A_0 = A_1 = 0.05, \zeta = 0.8, \omega = \pi/4$, $M = Da = 1, \mathrm{Pr} = 21$, and $t = 1$.

Conversely, Figure 7 demonstrates that an elevation in the Prandtl number (Pr) results in a reduction in both velocity and temperature profiles. Increasing the Prandtl number results in higher momentum diffusivity and viscosity for the fluid while its thermal diffusivity decreases. Thus, viscous force dominates the thermal diffusivity, increasing fluid motion's friction. Hence, fluid velocity decreases. A higher Prandtl number will let the fluid cool down faster since the heat diffuses rapidly. Consequently, the fluid temperature falls. In conclusion, the Prandtl number's effect on the thermal behaviour and heat transfer properties of blood can have implications for blood flow dynamics and temperature distribution within the circulatory system.

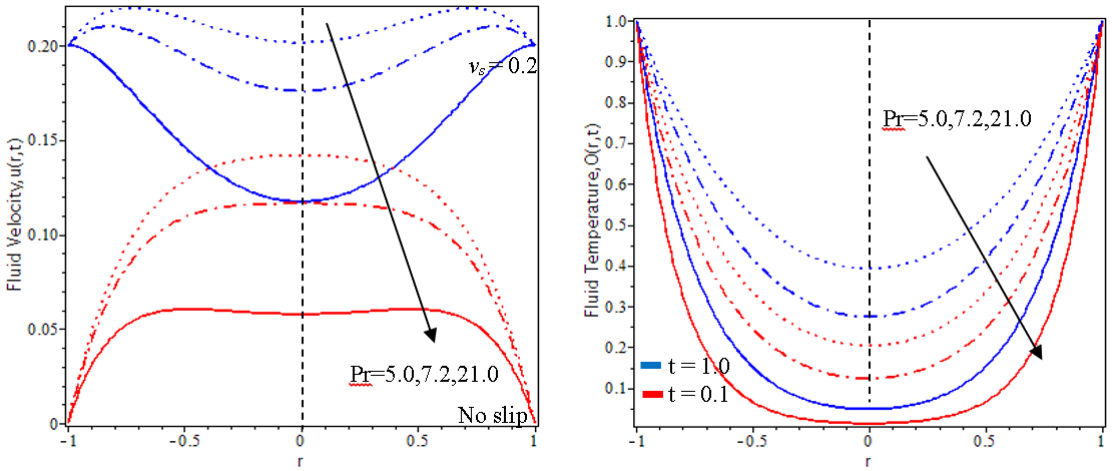

(a) Fluid velocity, $v(r,t)$ (b) Fluid temperature, $\theta(r,t)$

Figure 7: Result Prandtl number on (a) fluid velocity, $v(r,t)$ and (b) fluid temperature $\theta(r,t)$ when $\alpha = 0.5$.

The depiction of fluid velocity and temperature in Figure 8 showcases the impact of the fractional parameter, α. The figures illustrate that as the fractional parameters increase, both fluid temperature and velocity decrease within a shorter time $(t = 0.1)$, as depicted in Figures 8(b) and 8(c), respectively. In the meantime, during a more extended period, $t = 1.0$, fluid temperature and velocity rise as fractional parameters increase. There are disparities between small and large periods due to memory effects in fractional derivatives [43]. Besides, based on the graph trend increment as shown in Figure 8(b), it proves that the fractional fluid model $(0 < \alpha < 1)$ is more sensible compared to the classical fluid model $(\alpha = 1)$ as time increases.

Finally, the influence of the slip velocity can be seen in Figures 3 – 8. It is clearly shown that fluid velocity increases, especially at the cylinder's boundary $(r = 1)$, by increasing the slip velocity parameter. It results from the velocity differential between the fluid particles flowing through the solid boundary cylinder and its solid wall. Additionally, fluid velocity slightly declines as it approaches the cylinder's center $(r = 0)$. This is due to the thickening of the boundary layer and high viscous force as the central cylinder approaches. Considering slip velocity is vital in mathematical modeling as it closely reflects real-life applications, and the results show the differences between slip and no-slip effects. In summary, higher slip velocity diminishes blood flow resistance, promoting greater volumetric flow rate and axial velocity within arteries, which is significant for physiological blood circulation regulation.

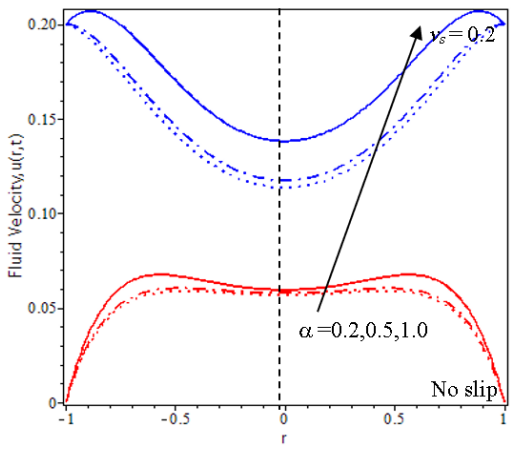

(a) Fluid velocity, $v(r,t)$ varies with slip velocity

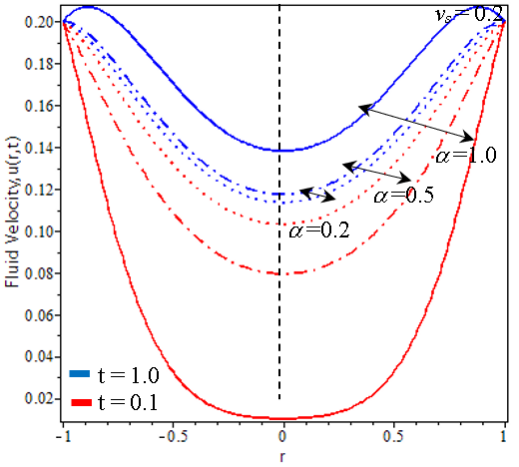

(b) Fluid velocity, $v(r,t)$ varies with time parameter

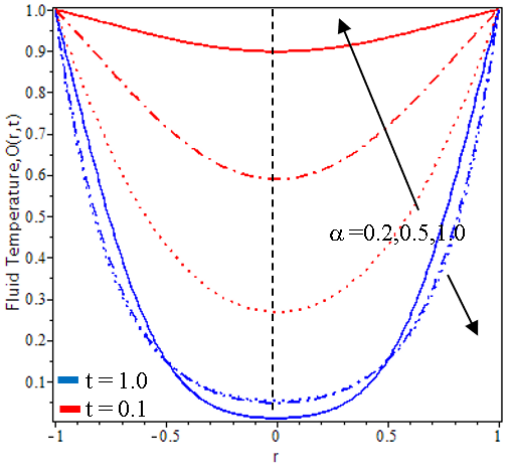

(c) Fluid temperature, $\theta(r,t)$

Figure 8: Result fractional parameter on (a) fluid velocity, $v(r,t)$ varies with slip velocity, (b) fluid velocity, $v(r,t)$ varies with time parameter and (c) fluid temperature, $\theta(r,t)$ when Pr=21.

Table 1 provides a summary of the Nusselt number and various factors, including the Prandtl number (Pr), time (t), and fractional parameter (α). It discovers that the Nusselt number rises when Pr grows. Meanwhile, the Nusselt number declines when α and t increase. Similar results of the Nusselt number are obtained by [6, 51]. Generally, viscous diffusion is dominant as the Prandtl number increases. It enhances convective heat transport and hence the Nusselt number. Furthermore, skin friction is shown in Table 2 for various physical factors, including the Prandtl number Pr, magnetic parameter M, Grashof number Gr, Darcy number Da, and Casson parameter ζ, slip velocity v_s, fractional parameter α, and time t. It shows that increment of skin friction as t, Gr, Da, ζ, and α increase while decrementing when Pr, M, and v_s growth. Larger skin friction indicates a larger resistant force exerted between moving fluid and the surface [51].

Table 1: Various parameters associated with the Nusselt number.

t	Pr	α	Nu	results
0.50	7.00	0.50	2.337	-
1.00	7.00	0.50	1.795	$\downarrow$
0.50	21.00	0.50	4.436	$\uparrow$
0.50	7.00	0.99	1.581	$\downarrow$

Table 2: Various parameters associated with skin friction.

t	Pr	M	Gr	Da	β	v_s	α	τ	results
0.50	7.00	1.00	1.00	1.00	0.80	0.50	0.50	-1.309	-
1.00	7.00	1.00	1.00	1.00	0.80	0.50	0.50	-0.976	$\uparrow$
0.50	21.00	1.00	1.00	1.00	0.80	0.50	0.50	-1.573	$\downarrow$
0.50	7.00	2.00	1.00	1.00	0.80	0.50	0.50	-1.816	$\downarrow$
0.50	7.00	1.00	2.00	1.00	0.80	0.50	0.50	-0.427	$\uparrow$
0.50	7.00	1.00	1.00	2.00	0.80	0.50	0.50	-1.021	$\uparrow$
0.50	7.00	1.00	1.00	1.00	1.20	0.50	0.50	-0.942	$\uparrow$
0.50	7.00	1.00	1.00	1.00	0.80	1.00	0.50	-3.638	$\downarrow$
0.50	7.00	1.00	1.00	1.00	0.80	0.50	0.99	-0.809	$\uparrow$

6 Conclusion

A through examination was conducted to study the properties of a Casson fluid in the context of free convection flow around a cylindrical object. The results of this investigation have been further expounded upon. Studying the behaviour of Casson fluid within a cylindrical structure is significant in biomedical applications since it mimics the flow characteristics of human blood in small arterial vessels. Both a magnetic field and porosity (similar to the cholesterol effect) influence the movement of the fluid. Besides, the impact of the pulsatile pressure gradient and slip boundary condition is also considered. These effects are crucial in designing the mathematical modeling as close to the physical problem. Blood flow, driven by the pulsating action of the heart, is indicated by the pulsatile pressure gradient, and the slip boundary represents the actual condition of the artery wall. The governing equation integrates the Caputo-Fabrizio fractional derivative. It is a non-singular kernel operator that is easier to handle for complicated problems. It is significant in its increased realism and accuracy compared to the classical model. Combining the Laplace transform and the finite Hankel transform yields the solution to the fractional dimensionless equation. The validity of the analytical result is confirmed by doing a comparative analysis with both the limiting case and previously published literature findings. The graphical representation displays the velocity and temperature profiles and their respective characteristics. Based on the empirical evidence, it may be inferred that:

- Increases of ζ lead to enhancing the fluid flow with the presence of the slip boundary when $t = 1.0$; meanwhile, fluid velocity declines for the no-slip condition at $t = 1.0$ and both slip and no-slip conditions at $t = 10.0$.
- The fluid velocity increase factors are Da, Gr, v_s, and t.
- Rise in the value of M and Pr causes a decrement in the fluid velocity.

- An elevation in the Prandtl number leads to a reduction in the temperature of the fluid.
- Higher fluid velocity and temperature over an extended period result from an increase in the fractional parameter, and the reverse is equally valid.
- The fluid model with fractional derivatives is a more accurate representation compared to the traditional fluid model.
- The cylinder's wall is seen to be impacted by the slip velocity.
- Increment of the Nusselt number due to Pr and decrement of the Nusselt number due to α and t.
- The skin friction rises due to t, Gr, Da, ζ, and α, while skin friction falls due to Pr, M, and v_s.

The present study considered that no slip temperature occurred. The study can be extended by considering the slip temperature to be more practical. Additionally, the influence of thermal radiation and chemical reactions can be regarded as to advance this investigation. Besides that, other fluids that mimic blood flow in a different situation can be considered, such as Herschel-Bulkley, Jeffrey fluid, and nanofluid.

Acknowledgement Special thanks to the Higher Education Ministry of Malaysia and the Research Management Centre (RMC) at UTM, their invaluable financial support through votes Q.J130000.3854.23H22 (UTMFR). The authors also express deep appreciation to all diligent researchers and friends who have reviewed and provided valuable suggestions to enhance the quality of this article.

Conflicts of Interest The authors declare that there is no conflict of interest regarding the publication of this article.

References

[1] M. Abd El-Aziz & A. S. Yahya (2017). Perturbation analysis of unsteady boundary layer slip flow and heat transfer of Casson fluid past a vertical permeable plate with Hall current. *Applied Mathematics and Computation*, *307*, 146–164. https://doi.org/10.1016/j.amc.2017.02.034.

[2] S. Abdalla, S. S. Al-Ameer & S. H. Al-Magaishi (2010). Electrical properties with relaxation through human blood. *Biomicrofluidics*, *4*(3), Article ID: 034101. https://doi.org/10.1063/1.3458908.

[3] T. N. Abdelhameed (2021). Entropy generation analysis for MHD flow of water past an accelerated plate. *Scientific Reports*, *11*(1), Article ID: 11964. https://doi.org/10.1038/s41598-021-89744-w.

[4] N. J. Alderman (1977). *Non-Newtonian Fluids: Guide to Classification and Characteristics*. Pipelines, London.

[5] F. Ali, A. Imtiaz, I. Khan & N. A. Sheikh (2018). Flow of magnetic particles in blood with isothermal heating: A fractional model for two-phase flow. *Journal of Magnetism and Magnetic Materials*, *456*, 413–422. https://doi.org/10.1016/j.jmmm.2018.02.063.

[6] F. Ali, A. Imtiaz, I. Khan, N. A. Sheikh & D. L. C. Ching (2018). Hemodynamic flow in a vertical cylinder with heat transfer: Two-phase Caputo Fabrizio fractional model. *Journal of Magnetics*, *23*(2), 179–191. http://dx.doi.org/10.4283/JMAG.2018.23.2.179.

[7] F. Ali, N. Khan, A. Imtiaz, I. Khan & N. A. Sheikh (2019). The impact of magnetohydrodynamics and heat transfer on the unsteady flow of Casson fluid in an oscillating cylinder via integral transform: A Caputo–Fabrizio fractional model. *Pramana*, *93*(3), Article ID: 47. https://doi.org/10.1007/s12043-019-1805-4.

[8] F. Ali, N. A. Sheikh, I. Khan & M. Saqib (2017). Magnetic field effect on blood flow of Casson fluid in axisymmetric cylindrical tube: A fractional model. *Journal of Magnetism and Magnetic Materials*, *423*, 327–336. https://doi.org/10.1016/j.jmmm.2016.09.125.

[9] J. P. M. Anurag & A. K. Singh (2021). Significance of time–dependent magnetohydrodynamic transient free convective flow in vertical annuli: An analytical approach with the finite Hankel transform. *Heat Transfer*, *50*(7), 6719–6736. https://doi.org/10.1002/htj.22200.

[10] J. P. M. Anurag & A. K. Singh (2021). Role of heat source/sink in transient free convective flow through a vertical cylinder filled with a permeable medium: An analytical approach. *Heat Transfer*, *50*(4), 3154–3175. https://doi.org/10.1002/htj.22022.

[11] D. Baliga, M. Gudekote, R. Choudhari, H. Vaidya & K. V. Prasad (2019). Influence of velocity and thermal slip on the peristaltic transport of a Herschel-Bulkley fluid through an inclined porous tube. *Journal of Advanced Research in Fluid Mechanics and Thermal Sciences*, *56*(2), 195–210.

[12] F. E. G. Bouzenna, M. T. Meftah & M. Difallah (2020). Application of the Caputo–Fabrizio derivative without singular kernel to fractional Schrödinger equations. *Pramana*, *94*(1), Article ID: 92.

[13] A. J. Chamkha (1997). Non-Darcy fully developed mixed convection in a porous medium channel with heat generation/absorption and hydromagnetic effects. *Numerical Heat Transfer, Part A Applications*, *32*(6), 653–675. https://doi.org/10.1080/10407789708913911.

[14] A. J. Chamkha (2000). Unsteady laminar hydromagnetic fluid–particle flow and heat transfer in channels and circular pipes. *International Journal of Heat and Fluid Flow*, *21*(6), 740–746. https://doi.org/10.1016/S0142-727X(00)00031-X.

[15] A. J. Chamkha, T. Groşan & I. Pop (2002). Fully developed free convection of a micropolar fluid in a vertical channel. *International Communications in Heat and Mass Transfer*, *29*(8), 1119–1127. https://doi.org/10.1016/S0735-1933(02)00440-2.

[16] R. P. Chhabra (2010). *Rheology of Complex Fluids*, chapter Non-Newtonian Fluids: An Introduction, pp. 3–34. Springer, New York. https://doi.org/10.1007/978-1-4419-6494-6_1.

[17] R. Choudhari, M. Gudekote, H. Vaidya & K. V. Prasad (2018). Peristaltic flow of Herschel-Bulkley fluidin an elastic tube with slip at porous walls. *Journal of Advanced Research in Fluid Mechanics and Thermal Sciences*, *52*(1), 63–75.

[18] R. K. Dash, K. N. Mehta & G. Jayaraman (1996). Casson fluid flow in a pipe filled with a homogeneous porous medium. *International Journal of Engineering Science*, *34*(10), 1145–1156. https://doi.org/10.1016/0020-7225(96)00012-2.

[19] M. Dehbani, M. Rahimi & Z. Rahimi (2022). A review on convective heat transfer enhancement using ultrasound. *Applied Thermal Engineering*, *208*, Article ID: 118273. https://doi.org/10.1016/j.applthermaleng.2022.118273.

[20] M. El-Shahed (2003). Pulsatile flow of blood through a stenosed porous medium under periodic body acceleration. *Applied Mathematics and Computation*, *138*(2-3), 479–488. https://doi.org/10.1016/S0096-3003(02)00164-9.

[21] M. F. Faraloya, S. Shafie, F. M. Siam, R. Mahmud & S. O. Ajadi (2021). Numerical simulation and optimization of radiotherapy cancer treatments using the Caputo fractional derivative. *Malaysian Journal of Mathematical Sciences*, *15*(2), 161–187.

[22] A. S. Hamarsheh, F. A. Alwawi, H. T. Alkasasbeh, A. M. Rashad & R. Idris (2020). Heat transfer improvement in MHD natural convection flow of graphite oxide/carbon nanotubes-methanol based casson nanofluids past a horizontal circular cylinder. *Processes*, *8*(11), Article ID: 1444. https://doi.org/10.3390/pr8111444.

[23] T. Hayat, M. Farooq & A. Alsaedi (2015). Thermally stratified stagnation point flow of Casson fluid with slip conditions. *International Journal of Numerical Methods for Heat & Fluid Flow*, *25*(4), 724–748. https://doi.org/10.1108/HFF-05-2014-0145.

[24] F. G. Hirsch, E. C. Texter, L. A. Wood, W. C. Ballard, F. E. Horan & I. S. Wright (1950). The electrical conductivity of blood: I. Relationship to erythrocyte concentration. *Blood*, *5*(11), 1017–1035. https://doi.org/10.1182/blood.V5.11.1017.1017.

[25] S. Husain, M. Adil, M. Arqam & B. Shabani (2021). A review on the thermal performance of natural convection in vertical annulus and its applications. *Renewable and Sustainable Energy Reviews*, *150*, Article ID: 111463. https://doi.org/10.1016/j.rser.2021.111463.

[26] M. Jalil & W. Iqbal (2021). Numerical analysis of suction and blowing effect on boundary layer slip flow of Casson fluid along with permeable exponentially stretching cylinder. *AIP Advances*, *11*(3), Article ID: 035304. https://doi.org/10.1063/5.0042314.

[27] D. F. Jamil, S. Saleem, R. Roslan, F. S. Al-Mubaddel, M. Rahimi-Gorji, A. Issakhov & S. U. Din (2021). Analysis of non-Newtonian magnetic Casson blood flow in an inclined stenosed artery using Caputo-Fabrizio fractional derivatives. *Computer Methods and Programs in Biomedicine*, *203*, 106044. https://doi.org/10.1016/j.cmpb.2021.106044.

[28] D. F. Jamil, S. Uddin & R. Roslan (2020). The effects of magnetic Casson blood flow in an inclined multi-stenosed artery by using Caputo–Fabrizio fractional derivatives. *Journal of Advanced Research in Materials Sciences*, *1*(1), 15–30.

[29] M. Javaid, M. Imran, M. A. Imran, I. Khan & K. S. Nisar (2020). Natural convection flow of a second grade fluid in an infinite vertical cylinder. *Scientific Reports*, *10*(1), Article ID: 8327. https://doi.org/10.1038/s41598-020-64533-z.

[30] B. K. Jha, S. B. Joseph & A. O. Ajibade (2022). Role of diffusion thermo on unsteady natural convection of a chemically reactive fluid impacted by heat source/sink in a tube. *Journal of Taibah University for Science*, *16*(1), 495–504. https://doi.org/10.1080/16583655.2022.2078135.

[31] A. R. A. Khaled & K. Vafai (2003). The role of porous media in modeling flow and heat transfer in biological tissues. *International Journal of Heat and Mass Transfer*, *46*(26), 4989–5003. https://doi.org/10.1016/S0017-9310(03)00301-6.

[32] I. Khan, N. Ali Shah, A. Tassaddiq, N. Mustapha & S. A. Kechil (2018). Natural convection heat transfer in an oscillating vertical cylinder. *PLoS One*, *13*(1), Article ID: e0188656. https://doi.org/10.1371/journal.pone.0188656.

[33] M. V. Krishna & A. J. Chamkha (2020). Hall and ion slip effects on unsteady MHD convective rotating flow of nanofluids–application in biomedical engineering. *Journal of the Egyptian Mathematical Society*, *28*(1), Article ID: 1. https://doi.org/10.1186/s42787-019-0065-2.

[34] B. Kumar, G. S. Seth, R. Nandkeolyar & A. J. Chamkha (2019). Outlining the impact of induced magnetic field and thermal radiation on magneto-convection flow of dissipative fluid. *International Journal of Thermal Sciences*, *146*, Article ID: 106101. https://doi.org/10.1016/j.ijthermalsci.2019.106101.

[35] G. Kumar & S. Rizvi (2021). Casson fluid flow past on vertical cylinder in the presence of chemical reaction and magnetic field. *Applications and Applied Mathematics: An International Journal* (*AAM*), *16*(1), Article ID: 28.

[36] R. A. Mahdi, H. A. Mohammed, K. M. Munisamy & N. H. Saeid (2015). Review of convection heat transfer and fluid flow in porous media with nanofluid. *Renewable and Sustainable Energy Reviews*, *41*, 715–734. https://doi.org/10.1016/j.rser.2014.08.040.

[37] S. Maiti, S. Shaw & G. C. Shit (2020). Caputo–fabrizio fractional order model on MHD blood flow with heat and mass transfer through a porous vessel in the presence of thermal radiation. *Physica A: Statistical Mechanics and its Applications*, *540*, Article ID: 123149. https://doi.org/10.1016/j.physa.2019.123149.

[38] S. Maiti, S. Shaw & G. C. Shit (2021). Fractional order model for thermochemical flow of blood with Dufour and Soret effects under magnetic and vibration environment. *Colloids and Surfaces B: Biointerfaces*, *197*, Article ID: 111395. https://doi.org/10.1016/j.colsurfb.2020.111395.

[39] S. Maiti, S. Shaw & G. C. Shit (2021). Fractional order model of thermo-solutal and magnetic nanoparticles transport for drug delivery applications. *Colloids and Surfaces B: Biointerfaces*, *203*, Article ID: 111754. https://doi.org/10.1016/j.colsurfb.2021.111754.

[40] O. U. Mehmood, N. Mustapha & S. Shafie (2012). Unsteady two-dimensional blood flow in porous artery with multi-irregular stenoses. *Transport in Porous Media*, *92*(2), 259–275. https://doi.org/10.1007/s11242-011-9900-0.

[41] A. J. Moitoi & S. Shaw (2023). Erratum: Magnetic drug targeting during Caputo fractionalized blood flow through permeable vessel. *Microvascular Research*, *148*. https://doi.org/10.1016/j.mvr.2023.104542.

[42] J. Nandal, S. Kumari & R. Rathee (2019). The effect of slip velocity on unsteady peristalsis MHD blood flow through a constricted artery experiencing body acceleration. *International Journal of Applied Mechanics and Engineering*, *24*(3), 645–659. https://doi.org/10.2478/ijame-2019-0040.

[43] G. A. M. B. Nchama (2020). Properties of Caputo–Fabrizio fractional operators. *New Trends in Mathematical Sciences*, *8*(1), 1–25.

[44] Y. Nubar (1971). Blood flow, slip, and viscometry. *Biophysical Journal*, *11*(3), 252–264. https://doi.org/10.1016/S0006-3495(71)86212-4.

[45] R. Padma, R. Ponalagusamy & R. T. Selvi (2019). Mathematical modeling of electro hydrodynamic non-Newtonian fluid flow through tapered arterial stenosis with periodic body acceleration and applied magnetic field. *Applied Mathematics and Computation*, *362*, Article ID: 124453. https://doi.org/10.1016/j.amc.2019.05.024.

[46] R. Padma, R. T. Selvi & R. Ponalagusamy (2019). Effects of slip and magnetic field on the pulsatile flow of a Jeffrey fluid with magnetic nanoparticles in a stenosed artery. *The European Physical Journal Plus*, *134*(5), Article ID: 221. https://doi.org/10.1140/epjp/i2019-12538-9.

[47] I. J. Rao & K. R. Rajagopal (1999). The effect of the slip boundary condition on the flow of fluids in a channel. *Acta Mechanica*, *135*(3), 113–126. https://doi.org/10.1007/BF01305747.

[48] M. V. S. Rao, K. Gangadhar & P. L. N. Varma (2020). Axisymmetric slip flow of a Powell-Eyring fluid due to induced magnetic field. *Malaysian Journal of Mathematical Sciences*, *14*(1), 95–114.

[49] V. P. Rathod & S. Tanveer (2009). Pulsatile flow of couple stress fluid through a porous medium with periodic body acceleration and magnetic field. *Bulletin of the Malaysian Mathematical Sciences Society*, *32*(2), 245–259.

[50] S. S. Ray, A. Atangana, S. C. Noutchie, M. Kurulay, N. Bildik & A. Kilicman (2014). Fractional calculus and its applications in applied mathematics and other sciences. *Mathematical Problems in Engineering*, *2014*(1), Article ID: 849395. https://doi.org/10.1155/2014/849395.

[51] R. Reyaz, A. Q. Mohamad, Y. J. Lim, M. Saqib & S. Shafie (2022). Analytical solution for impact of Caputo–Fabrizio fractional derivative on MHD casson fluid with thermal radiation and chemical reaction effects. *Fractal and Fractional*, *6*(1), 38. https://doi.org/10.3390/fractalfract6010038.

[52] D. S. Sankar & A. Ismail (2009). Two–fluid mathematical models for blood flow in stenosed arteries: A comparative study. *Boundary Value Problems*, *2009*, Article ID: 568657. https://doi.org/10.1155/2009/568657.

[53] N. Sene (2022). Analytical solutions of a class of fluids models with the Caputo fractional derivative. *Fractal and Fractional*, *6*(1), Article ID: 35. https://doi.org/10.3390/fractalfract6010035.

[54] A. Shaikh, A. Tassaddiq, K. S. Nisar & D. Baleanu (2019). Analysis of differential equations involving Caputo–Fabrizio fractional operator and its applications to reaction–diffusion equations. *Advances in Difference Equations*, *2019*(1), Article ID: 178. https://doi.org/10.1186/s13662-019-2115-3.

[55] T. Sochi (2010). Non-Newtonian flow in porous media. *Polymer*, *51*(22), 5007–5023. https://doi.org/10.1016/j.polymer.2010.07.047.

[56] H. J. Xu, Z. B. Xing, F. Q. Wang & Z. M. Cheng (2019). Review on heat conduction, heat convection, thermal radiation and phase change heat transfer of nanofluids in porous media: Fundamentals and applications. *Chemical Engineering Science*, *195*, 462–483. https://doi.org/10.1016/j.ces.2018.09.045.

[57] H. B. Yadeta & S. Shaw (2023). Magnetic drug targeting during Casson blood flow in a microvessel: A Caputo fractional model. *Journal of Magnetism and Magnetic Materials*, *568*, Article ID: 170363. https://doi.org/10.1016/j.jmmm.2023.170363.

[58] D. R. Yanala, A. K. Mella, S. R. Vempati & B. S. Goud (2021). Influence of slip condition on transient laminar flow over an infinite vertical plate with ramped temperature in the presence of chemical reaction and thermal radiation. *Heat Transfer*, *50*(8), 7654–7671. https://doi.org/10.1002/htj.22247.